

Calculation of strongly-coupled rotational bands in terms of the tilted axis cranking model

Shin-Ichi Ohtsubo and Yoshifumi R. Shimizu

Department of Physics, Kyushu University, Fukuoka 812-8581, Japan

Abstract

Recently observed strongly-coupled rotational bands associated with the $\nu[505]_{\frac{11}{2}}^{-}$ quasiparticle state are studied by means of a microscopic tilted axis cranking (TAC) model. The results of calculation for the routhians and the $B(M1)/B(E2)$ ratios are investigated in the light of other existing models, i.e. the strong-coupling model and the conventional cranking model. It is demonstrated that only the TAC model can successfully reproduce these two observables at the same time. The reason of the success is clarified by making connections between these models.

PACS number(s): 21.60.-n

keywords: High- K rotational band; Tilted axis cranking; Cranked shell model; $B(M1)/B(E2)$

1 Introduction

Bohr-Mottelson's strong-coupling model [1] is the first pioneering work which is capable to describe interplay between the collective and the single-particle rotational motions in well-deformed nuclei. It successfully reproduce both the energy spectra and the electromagnetic transition properties of rotational bands in odd nuclei. It is, however, of phenomenological nature since essential quantities like the moment of inertia and the quadrupole moment are model-parameters and are adjusted in comparison with experimental data. One has to combine it with a more microscopic model such as the Nilsson single-particle model. Another drawback of the model is that it is based on the adiabatic assumption of the collective rotation and the application to the high angular momentum regime is not straightforward. The particle-rotor model [1, 2] is a possible means to extend the idea by lifting the adiabatic assumption and including the effect of Coriolis coupling by exact diagonalization, although it is still semi-phenomenological in the sense that the macroscopic "rotor" part is explicitly introduced. Nowadays, fully microscopic approaches are available, for example, the variation after full angular momentum projection base on the generalized mean-field [3] and the projected shell model [4]. However, they are very complicated and lose simplicity of the model.

On the other hand, by taking into account the effect of rotation unperturbatively, the mean-field theory has been extended in the rotating frame: The cranking model or the Cranked Shell Model (CSM) [5], which is simple and yet microscopic, has been successfully applied to understand various high-spin phenomena [6] such as backbending of moment of inertia. Recently, this cranking model has been further extended in such a way to include the tilting degrees of freedom of rotation-axis relative to the deformed shape; the Tilted Axis Cranking (TAC) model [7, 8, 9] (the conventional cranking is called the Principal Axis Cranking (PAC) model, instead), which gives nice interpretations of new types of nuclear rotational motions, e.g. the shears bands [10] and the chiral bands [9, 11]. Although these cranking models treat the rotational motion in a semiclassical manner, its simplicity allows us to have a clear physical picture of various collective rotational motions, which are actually a result of the complex nuclear many-body problem.

The purpose of the present paper is two folds: The first is to give a clear relationship between the strong-coupling model and the TAC model. The second is to apply the TAC model to the

strongly-coupled high- K one-quasiparticle bands, which have been recently measured at JAERI up to high-spin states ($I \lesssim 22\hbar$) in several nuclei in the light rare earth region. In this way, it will be demonstrated that the TAC method is a powerful tool to investigate the high-spin phenomena, including not only such new types of rotational bands but also well-known typical rotational bands, and thus gives a good description of the nuclear rotational motions from low- to high-spin states.

In Section 2, the relation between the TAC model and the strong-coupling model is studied. The results of the TAC model are presented in Section 3 in comparison with the experimental data. Section 4 is devoted to the conclusion.

2 Relation between strong-coupling model and TAC model

Since the strong-coupling model is well-known [1], we only recapitulate the final expressions necessary for the following discussion. Our main object of study is rotational band of odd well-deformed axially symmetric nuclei with a valence nucleon occupying a high- K orbit. Therefore, we use the simplest expressions for the axially symmetric case without the decoupling terms, and higher order Coriolis coupling is neglected completely: The energy spectrum is given by¹

$$E_K(I) = \frac{1}{2\mathcal{J}} [I(I+1) - K^2] + E_K^0 - \frac{K}{2\mathcal{J}} \quad (I \geq K), \quad (1)$$

and the $E2$ and $M1$ transition probabilities are given by

$$B(E2; I \rightarrow I-2) = \frac{5}{16\pi} Q_0^2 \langle IK20 | I-2K \rangle^2, \quad (2)$$

$$B(M1; I \rightarrow I-1) = \frac{3}{4\pi} (g_K - g_R)^2 K^2 \langle IK10 | I-1K \rangle^2, \quad (3)$$

respectively. Here the introduced parameters are the moment of inertia, \mathcal{J} , the band head energy, E_K^0 , the quadrupole moment, Q_0 , and the intrinsic and rotational g -factors, g_K and g_R .

Details of the microscopic TAC model is given in Ref. [8, 9]. We follow these references and briefly discuss about what is necessary in the following discussion. As for the starting microscopic hamiltonian, we take the Nilsson single-particle potential [12] with the ls and l^2 parameters taken from Ref. [13], and the monopole pairing residual interaction. Thus, using the axial symmetry of the potential, the single-particle (two-dimensional) TAC hamiltonian is

$$\hat{h}' = \hat{h}_{\text{Nilss}} - \lambda \hat{N} - \Delta(\hat{P}^\dagger + \hat{P}) - (\omega_x \hat{J}_x + \omega_z \hat{J}_z), \quad (4)$$

where λ and Δ are the chemical potential and the pairing gap, \hat{N} , \hat{P}^\dagger and (\hat{J}_x, \hat{J}_z) are the number operator, the monopole pairing operator, and (x, z) -components of the angular momentum vector operator, respectively. The characteristic feature of the TAC model is the inclusion of the tilting degree of freedom of rotation-axis with respect to the principal axes (x, y, z) of the deformed shape, which is represented in the cranking term $-\boldsymbol{\omega} \hat{\mathbf{J}} = -(\omega_x \hat{J}_x + \omega_z \hat{J}_z)$. The (two-dimensional) components of the rotational frequency vector $\boldsymbol{\omega}$ are given by the rotational frequency ω and the tilting angle of the frequency vector θ_ω ;

$$\begin{cases} \omega_x = \omega \sin \theta_\omega, \\ \omega_z = \omega \cos \theta_\omega. \end{cases} \quad (5)$$

¹ We use $\hbar = 1$ unit throughout in this paper.

The expectation value of the angular momentum operators is related to the angular momentum quantum number I by

$$J \equiv \sqrt{\langle \hat{J}_x \rangle^2 + \langle \hat{J}_z \rangle^2} = I + \frac{1}{2}. \quad (6)$$

Here the shift $+\frac{1}{2}$ is due to the quantum correction of the rotational motion. Note that the rotational frequency ω in Eq. (5) is a conjugate variable of J , namely,

$$\omega = \frac{dE}{dJ} = \frac{dE}{dI}, \quad (7)$$

and the total routhian is defined by $E' = E - \omega J$. The tilting angle of the angular momentum vector is similarly defined as

$$\theta_J = \tan^{-1} \left(\frac{\langle \hat{J}_x \rangle}{\langle \hat{J}_z \rangle} \right) = \cos^{-1} \left(\frac{\langle \hat{J}_z \rangle}{J} \right). \quad (8)$$

This angle is determined at each rotational frequency by the selfconsistency condition: The routhian in the rotating frame is minimum (stationary) with respect to the angle of the frequency vector, which is equivalent to the condition that two tilting angles coincide:

$$\left. \frac{\partial E'}{\partial \theta_\omega} \right|_\omega = 0 \quad \iff \quad \theta_\omega = \theta_J. \quad (9)$$

Once the angle θ_ω , or θ_J , is determined at each rotational frequency, the routhian or the energy of the system is calculated according to the usual mean-field approximation as a function of the rotational frequency ω , or of the angular momentum $I = J - 1/2$, if necessary.

In the present paper, the monopole pairing gap, Δ , as well as the deformation parameters are kept constant, while the chemical potential is determined by the number condition. Then, in order to guarantee the condition (9), one has to use the following definition of the routhian,

$$E' = \langle \hat{h}_{\text{Nils}} \rangle - 2\Delta \langle \hat{P}^\dagger \rangle - \langle \omega \hat{J} \rangle, \quad (10)$$

in place of the usual definition,

$$E' = \langle \hat{h}_{\text{Nils}} \rangle - G \langle \hat{P}^\dagger \rangle^2 - \langle \omega \hat{J} \rangle, \quad (11)$$

where G is the strength of the monopole pairing interaction, and the pairing gap in this case is determined selfconsistently by $\Delta = G \langle \hat{P}^\dagger \rangle$.

The transition probabilities in the TAC model are given by [8]

$$B(E2; I \rightarrow I - 2) = \frac{5}{16\pi} \frac{3}{8} \left(\langle \hat{Q}_0 \rangle^2 \sin^2 \theta_J \right)^2, \quad (12)$$

$$B(M1; I \rightarrow I - 1) = \frac{3}{4\pi} \frac{1}{2} \left(\langle \hat{\mu}_z \rangle \sin \theta_J - \langle \hat{\mu}_x \rangle \cos \theta_J \right)^2, \quad (13)$$

where $\hat{Q}_0 = \sum_{a=1}^A (2\hat{z}^2 - \hat{x}^2 - \hat{y}^2)_a$, is the quadrupole moment operator around the z -axis, and $(\hat{\mu}_x, \hat{\mu}_z)$ is (x, z) -component of the magnetic moment vector operator, $\hat{\boldsymbol{\mu}} = \sum_{a=1}^A (g_l \hat{\boldsymbol{l}} + g_s^{\text{eff}} \hat{\boldsymbol{s}})_a$. Here the tilting angle θ_J appears and the expectation values of the operators in the body-fixed coordinate (x, y, z) are used. The following shape-consistency constraints should be satisfied at each frequency in order to define the body-fixed frame [14]:

$$\left\langle \sum_{a=1}^A (\hat{x}\hat{y})_a \right\rangle = \left\langle \sum_{a=1}^A (\hat{y}\hat{z})_a \right\rangle = \left\langle \sum_{a=1}^A (\hat{z}\hat{x})_a \right\rangle = 0. \quad (14)$$

In the present paper, however, we use the fixed frame defined at the zero frequency for simplicity. We have checked that the ratio $|\langle \sum_{a=1}^A (\hat{z}\hat{x})_a \rangle|/|\langle \hat{Q}_0 \rangle|$ is less than 5×10^{-3} at all rotational frequencies in the present calculations (other constraints are automatically satisfied because of the two-dimensional nature of the cranking term), and so we believe that the breaking of the shape-consistency does no harm.

The TAC prescription contains the conventional cranking (PAC) model as a limiting case: Taking the z -axis as a symmetry-axis and the x -axis as a rotation-axis, the PAC model is realized if the selfconsistently determined tilting angle is $\theta_J = 90^\circ$. The important difference of the TAC ($\theta_J \neq 90^\circ$) and PAC ($\theta_J = 90^\circ$) models is that the signature α , the eigenvalue of 180° -rotation about x -axis, is a good quantum number in the PAC while the signature symmetry is broken in the TAC. Thus the $M1$ transitions only occur between the signature partner bands, and the $B(M1)$ in the PAC model is calculated by [15, 16]

$$\begin{aligned} B\left(M1; (I, \alpha = -\frac{1}{2}) \longleftrightarrow (I \mp 1, \alpha = +\frac{1}{2})\right) \\ = \left| \left\langle \alpha = -\frac{1}{2} \left| \frac{1}{\sqrt{2}} \{i\mathcal{O}(M1, y) \pm \mathcal{O}(M1, z)\} \right| \alpha = +\frac{1}{2} \right\rangle \right|^2, \end{aligned} \quad (15)$$

with the transition operator

$$\mathcal{O}(M1, \nu) \equiv \sqrt{\frac{3}{4\pi}} (\hat{\mu}_\nu - \tilde{g}_R \hat{J}_\nu), \quad \tilde{g}_R = \langle \hat{\mu}_x \rangle_0 / \langle \hat{J}_x \rangle_0, \quad (16)$$

where $\langle * \rangle_0$ means that the expectation value is taken with respect to the zero-quasiparticle state (the even-even core state) at each rotational frequency. Note that the quantity \tilde{g}_R play a similar role as the rotational g -factor in Eq. (3), which comes from the effect of the rotational Nambu-Goldstone mode of even-even core nucleus [16].

Now it is the place to consider the relation between the strong-coupling model and the TAC model. As is discussed in Ref. [8], the TAC solution corresponding to the high- K rotational band starts to appear from the so-called ‘‘band head frequency’’ ω_{BH} ; namely as long as $\omega < \omega_{\text{BH}}$ the selfconsistent tilting angle stays at $\theta_J = 0^\circ$. In the strong coupling model, where the z -component of the angular momentum (the projection of angular momentum to the symmetry axis) is K , the angle between the the angular momentum vector and the symmetry axis can be introduced through

$$\theta_K(I) \equiv \cos^{-1}(K/J) = \cos^{-1}\left(\frac{K}{I + \frac{1}{2}}\right), \quad (17)$$

because of Eq. (6). Since the rotational frequency of the strong-coupling band (1) is given by $\omega_K(I) = \partial E_K / \partial I = (I + \frac{1}{2}) / \mathcal{J}$, the frequency corresponding to $\theta_K(I) = 0$ is [8]

$$\omega_{\text{BH}} = \frac{K}{\mathcal{J}} \quad (\text{strong-coupling model}). \quad (18)$$

This frequency may be compared with the band head frequency ω_{BH} in the TAC model calculation.

Next let us consider the transition probabilities. Using the asymptotic values ($I \gg 1$) of the Clebsch-Gordan coefficients [17, 18],

$$\langle IK20 | I - 2K \rangle \approx \sqrt{\frac{3}{8}} \left(1 - \left(\frac{K}{I - \frac{1}{2}} \right)^2 \right) = \sqrt{\frac{3}{8}} \sin^2 \theta_K(I - 1), \quad (19)$$

$$\langle IK10 | I - 1K \rangle \approx \sqrt{\frac{1}{2}} \sqrt{1 - \left(\frac{K}{I} \right)^2} = \sqrt{\frac{1}{2}} \sin \theta_K(I - \frac{1}{2}), \quad (20)$$

it is apparent that the expression of $B(E2)$ in the strong-coupling model (2) corresponds to the one in the TAC model (12) if the TAC tilting angle θ_J is identified with $\theta_K(I)$ in Eq. (17) at $I = I - 1$, the mean value of the initial and final angular momenta. As for the $B(M1)$, introducing g -factors similar to that in Eq. (16),

$$\bar{g}_K = \langle \hat{\mu}_z \rangle / \langle \hat{J}_z \rangle, \quad \bar{g}_R = \langle \hat{\mu}_x \rangle / \langle \hat{J}_x \rangle, \quad (21)$$

the quantity in the parenthesis in Eq. (13) is written as

$$\langle \hat{\mu}_z \rangle \sin \theta_J - \langle \hat{\mu}_x \rangle \cos \theta_J = (\bar{g}_K - \bar{g}_R) \langle \hat{J}_z \rangle \sin \theta_J, \quad (22)$$

which clearly indicates a equivalence between Eqs. (3) and (13) if the g -factors are the same, $\langle \hat{J}_z \rangle = K$, and θ_J are identified with $\theta_K(I)$ at $I = I - \frac{1}{2}$, again the mean value of the initial and final angular momenta. The effect of finite K -values in the Clebsch-Gordan coefficients has been recognized and similar correction terms to the formula in the PAC model have been used in Refs. [19, 20] for transition probabilities. For the high- K orbitals the Coriolis coupling is not effective even at the high-spin states, so that the signature splitting is very small. Then, the matrix element of $\mathcal{O}(M1, y)$ in Eq. (15) is expected to be vanishing [16], and the three expressions of $B(M1)$, Eqs. (3), (13), and (15) tends to coincide in the limit, $\theta_J = \theta_K(I) \rightarrow 90^\circ$, if all the g -factors are the same and $\langle \hat{J}_z \rangle_{\text{TAC}} = \langle \alpha = -\frac{1}{2} | \hat{J}_z | \alpha = +\frac{1}{2} \rangle_{\text{PAC}} = K$. We will see that this trend is observed for $B(M1)$ in the actual cases studied in the next section.

3 Results and discussions

In this section, the results of simplest TAC calculations are presented for high- K one-quasiparticle bands. It will be demonstrated that the TAC model is a powerful microscopic method to describe the strongly-coupled rotational bands up to high-spin states. Recently, rather systematic measurements, using the Coulomb excitation and the in-beam γ -ray spectroscopy, have been performed at JAERI (Japan Atomic Energy Research Institute) for stable neutron-odd nuclei around ^{155}Gd nucleus, ^{153}Sm [21, 22], ^{155}Gd [23], ^{157}Gd [25], ^{157}Dy [25] and ^{159}Dy [26] (see also the Nuclear Data [27]). In these series of experiments, both the positive- and negative-parity yrast bands have been identified up to high-spin states ($I \lesssim 25\hbar$). They are $\Delta I = 2$ aligned (weakly-coupled) rotational bands with signature $\alpha = \pm\frac{1}{2}$, and positive-parity (Band 1) and the negative-parity (Band 2) bands are supposed to be the one-quasiparticle bands associated with the Nilsson orbitals $\nu[651]_{\frac{3}{2}}^{+}$ and $\nu[521]_{\frac{3}{2}}^{-}$, respectively. In addition to these observations, a $\Delta I = 1$ strongly-coupled rotational sequence with negative-parity has also been measured up to high-spin states ($I \lesssim 22\hbar$), which is supposed to be based on the high- K $\nu[505]_{\frac{11}{2}}^{-}$ configuration.

We have applied the (two-dimensional) TAC model in §2 to these measured rotational bands. The results for the Band 1 and 2 give the selfconsistent tilting angle $\theta_J = 90^\circ$ even at lowest frequencies, and show rotationally aligned (decoupled) bands with signature-splitting, which is large for Band 1 and moderate for Band 2; namely, they are found to be well described in the conventional PAC model. Only the high- K (or high- Ω) $\nu h_{11/2}$ band has the selfconsistent tilting angle, $0 < \theta_J < 90^\circ$, in the observed rotational frequencies, corresponding to the observed signature-splitting that is negligibly small. In the following we mainly concentrate on this high- K band.

First, let us explain the details of the calculation: Assuming axially symmetric deformation ($\gamma = 0^\circ$), selfconsistent values of the Nilsson deformation parameters (ϵ_2, ϵ_4) of the ground state have been searched by using the Nilsson-Strutinsky method at zero rotational frequency, where the pairing correlations are included by using the smooth pair-gap method with $\tilde{\Delta} = 12/\sqrt{A}$ MeV. The

result, however, is found to give systematically smaller deformations compared to those deduced from the measured $B(E2)$ values near the ground state. Therefore we have multiplied calculated values of ϵ_2 by a factor 1.1 (keeping calculated ϵ_4 values) in all nuclei in order to reduce the discrepancy. The deformation parameters thus determined are listed in Table 1. These nuclei have rather stable deformation in the rotational frequency range under consideration, and therefore we have used fixed deformation parameters in all the following calculations. The pairing correlation is also an important factor to understand the properties of rotational bands. In the test calculation, we have used the pairing force parameter which gives the values of pairing gap corresponding to the measured third order even-odd mass differences [1] (the mean value of neighbouring even-even nuclei for neutron), and performed the selfconsistent pairing calculation (c.f. Eq. (11)), where the blocking effect is properly taken into account for neutrons. However, we have found that the moment of inertia is too small at low frequency and the pairing reduction at high frequency is too large. These trends have been known in the conventional PAC calculation for many years. Therefore, in order to compare the calculated results with experimental data, we have used the constant-pairing-gap calculations (c.f. Eq. (10)) with neutron and proton pairing gaps, Δ_ν and Δ_π , which are obtained by multiplying the factor 0.7 and 0.9, respectively, to the measured even-odd mass differences. Here the stronger reduction of the neutron gap is due to the fact that the selfconsistent blocking calculations for neutron one-quasiparticle states give about 80% reduction on average. Further reduction in both the neutron and proton gaps is to make the moment of inertia larger. The monopole pairing gap parameters thus determined and used in the following calculations are listed in Table 1. The dependence of the final result on these pairing gap parameters will be discussed in the end of this section.

In Fig. 1, the total routhian surfaces of the $\nu[505]_{\frac{11}{2}}^-$ bands in ^{157}Gd at rotational frequencies $\hbar\omega = 0.12, 0.24$ and 0.36 MeV are shown as functions of the tilting angle θ_ω . At $\theta_\omega = 90^\circ$, the TAC scheme reduces to the PAC scheme and the calculated states are classified by the signature quantum numbers $\alpha = \pm\frac{1}{2}$. It is, however, noticed that the signature classification is not appropriate for the high- K orbitals, for which the K -quantum number along the z -axis (symmetry axis) is conserved in a very good approximation and the signature splitting is negligible. In the figure, two surfaces shown by the full and dotted curves have been calculated diabatically starting from states at $\theta_\omega < 90^\circ$ and $\theta_\omega > 90^\circ$, respectively, and the two minima correspond to the TAC states with approximately good K -quantum number $+K > 0$ and $-K < 0$. From the symmetry with respect to the transformation $\theta_\omega \leftrightarrow 180^\circ - \theta_\omega$, they are symmetric with respect to $\theta_\omega = 90^\circ$. Note, however, that this diabatic tracing is of approximate nature valid only for the high- K orbitals, for which the Coriolis coupling between the conjugate states with $\pm K$ are negligible in the shown frequency range; if the same routhian surface is considered for the low- K alignable orbits, the signature splitting at $\theta_\omega = 90^\circ$ is sizable and the two adiabatic surfaces are separated into lower- and higher-energy surfaces (c.f. Ref. [8]). At $\hbar\omega = 0.12$ MeV, the selfconsistent solution has $\theta_\omega = 0^\circ$ or 180° , while, at $\hbar\omega = 0.24$ (0.36) MeV, the selfconsistent tilting angle becomes $\theta_\omega \approx 60^\circ$ (80°) or 120° (100°). Namely, the selfconsistent TAC solutions stay energetically favoured compared to the conventional PAC solutions with $\theta_\omega = 90^\circ$ by about 300 – 400 keV in this case.

Now let us discuss the calculated routhians in comparison with experimental data, which are summarized in Fig. 2. In the figure the relative routhians of Band 1, Band 2, and the $\nu[505]_{\frac{11}{2}}^-$ band are shown as functions of the rotational frequency in each nucleus (Band 1 was not observed in ^{153}Sm); the origin of the calculated routhians are chosen mainly to reproduce Band 1. Note that the frequency ω is defined in Eq. (7), which is different from the conventional PAC scheme, see discussion below. We take a simple reference band with a constant moment of inertia \mathcal{J}_0 (“rigid-body reference” for each nucleus), which roughly corresponds to the ground state band in the neighbouring even-even nuclei. Here we have to use a different \mathcal{J}_0 value for calculated routhians: This is because our calculated moment of inertia is still smaller, even though somewhat reduced pairing gaps are used.

The \mathcal{J}_0 values used for calculated routhians are 10% smaller than those for experimental routhians in all nuclei, which gives overall agreements between them. The actual values of \mathcal{J}_0 used to make the figure are listed in Table 1. This factor is consistent with the known fact that the moment of inertia is generally underestimated by about 20–30% if only the monopole pairing interaction, which reproduces the experimental even-odd mass differences, is properly included [28]. One may be able to avoid such a phenomenological adjustment if the quadrupole pairing interaction is included (see, e.g. [29]). As already mentioned the selfconsistent tilting angle is $\theta_J = 90^\circ$ in Band 1 and 2, so that they are in fact the PAC bands and have appreciable signature splittings. In contrast, the $\nu[505]_{\frac{11}{2}}^-$ band is strongly-coupled band and exhibits no signature splitting in the observed frequency range. In the $N = 91$ isotones, the $\nu h_{11/2}$ band is located between Band 1 and Band 2, while, in the $N = 93$ isotones, it is above the Band 1. The calculation successfully reproduces this feature. In the $N = 91$ isotones, the effect of the $i_{13/2}$ two-neutron alignment is seen in the calculated routhians of Band 2 and the $\nu h_{11/2}$ band, but no clear indication is observed in the experimental routhian. Therefore it is suggested that the alignment is delayed or the interband interaction is larger than the calculated one. The routhian of Band 2 is slightly lower in the $N = 91$ isotones, while it is slightly higher in ^{157}Gd . Although there are some discrepancies we suppose that the overall agreement is satisfactory considering that the model parameters are not adjusted in each nucleus.

As it is discussed in Ref. [8], strongly-coupled high- K bands may possibly be treated in the PAC model, i.e. in the conventional cranked shell model, if the constancy of K quantum number is good. It should, however, be noted that the rotational frequency in the PAC model is “the collective rotational frequency” (the x -component of the angular frequency vector) in contrast to Eq. (7) in the TAC treatment;

$$\omega_x = \frac{dE}{dI_x} \quad \text{with} \quad I_x(I) \equiv \sqrt{(I + \frac{1}{2})^2 - K^2}, \quad (23)$$

where the z -component of angular momentum is assumed to be constant K . Then, $\omega_x/\omega = I_x/J$, which leads again $\theta_\omega = \theta_J$. Correspondingly, equivalent routhians in the PAC scheme are those in “the collectively rotating frame” defined by $E'_x = E - \omega_x I_x$. Thus the two states with the same frequency in the TAC and PAC schemes have quite different angular momenta from each other if K is large. The two routhians corresponding to ω and ω_x for the simple strong-coupling spectra (1) are

$$\text{strong-coupling case : } \begin{cases} E'(\omega) = -\frac{1}{2}\mathcal{J}\omega^2 - \frac{K^2}{2\mathcal{J}} + E_K^0, \\ E'_x(\omega_x) = -\frac{1}{2}\mathcal{J}\omega_x^2 + E_K^0, \end{cases} \quad (24)$$

where $E_K^0 = E_K^0 - (K + \frac{1}{4})/2\mathcal{J}$. Thus, if two routhians, (ω, E') and (ω_x, E'_x) , are plotted in the same figure, the former is shifted by $-K^2/2\mathcal{J}$ relative to the latter. The energy difference between the TAC and PAC (90° tilting angle) states in Fig. 1 is about 300 – 400 keV, and can be interpreted in this way. These TAC and PAC treatments for the $\nu[505]_{\frac{11}{2}}^-$ band are compared in Fig. 3; the solid line and triangles are the calculated and experimental routhians in the TAC scheme, and the dashed line and circles are the calculated and experimental routhians in the PAC scheme. The TAC scheme routhian for the strong-coupling expression (24) calculated by employing the moment of inertia which fits the experimental spectra (see Table 2) is also included in the figure as the dot-dashed line. As is stressed in Ref. [8] the two schemes are not strictly equivalent because the assumption of the constant $K = \langle J_z \rangle$ is not valid in the selfconsistent TAC calculations, thus the PAC scheme is only an approximation of the TAC scheme. In fact, as is clearly seen in Fig. 3, the calculated as well as the experimental routhians in the two schemes are not strictly parallel, especially at high-spin region; the distance between them gets smaller at higher frequency, indicating that $\langle J_z \rangle$ reduces

sizably. However, the degree of agreement between the calculations and data are similar in the two schemes.² This result suggests that the change of $\langle J_z \rangle$ is not enough to show the breakdown of the PAC scheme in this $\nu[505]_{\frac{11}{2}}^-$ band. Nevertheless, the simple strong-coupling energy (1) does not give a good approximation; the change of moment of inertia as a function of the rotational frequency and the effect of the alignments are very important to understand the high-spin spectra, which are taken care of by both the TAC and PAC methods.

In addition to the energy spectra, the $B(M1)/B(E2)$ ratios have been also measured in the JAERI experiments. We compare the results of the calculation with experimental data for the $\nu[505]_{\frac{11}{2}}^-$ band in Fig. 4 (no $B(M1)/B(E2)$ data are available in ^{153}Sm and ^{157}Gd). The selfconsistently determined the tilting angle θ_J and the experimentally deduced angle $\theta_K(I)$ based on Eq. (17) are also included in the figure. As for the effective g -factors, g_s^{eff} , 0.7 times the free values [30] are used in the calculation of $B(M1)$. The results of TAC calculation reproduce the experimental data reasonably well, although the alignment of two-quasineutrons, which occurs at lower frequency than the data, makes the $B(M1)$ too small at highest frequencies. As increasing the rotational frequency, the $B(M1)/B(E2)$ ratio decreases, which is qualitatively understood by the strong-coupling expressions (2) and (3), or by using the asymptotic relations (19) and (20) the ratio can be further written as [31, 23],³

$$\frac{B(M1; I \rightarrow I-1)}{B(E2; I \rightarrow I-2)} = \frac{12}{5} \left[\frac{(g_K - g_R)K}{Q_0} \right]^2 \frac{\langle IK10|I-1K \rangle^2}{\langle IK20|I-2K \rangle^2}, \quad (25)$$

$$\approx \frac{16}{5} \left[\frac{(g_K - g_R)K}{Q_0} \right]^2 \frac{\sin^2 \theta_K(I - \frac{1}{2})}{\sin^4 \theta_K(I - 1)}. \quad (26)$$

In the figure the ratio estimated by using the strong-coupling expression (25) is also included as the dashed line for ^{155}Gd and $^{157,159}\text{Dy}$, where the parameter $[(g_K - g_R)K/Q_0]^2$ is fitted to the data. As it is clear in Eqs.(26), the ratio is quite sensitive to the geometry of the angular momentum vector in the body-fixed frame. In terms of the TAC scheme, the vector of the total angular momentum is orienting toward the x -axis (the axis of collective rotation) from the z -axis (the symmetry axis) as increasing the rotational frequency. From the functional form of the angle one can estimate the band head frequency ω_{BH} , that is determined by the value at which the angle starts to non-zero degree. Using θ_J and $\theta_K(I)$ one obtains the calculated and experimental ω_{BH} , respectively. Furthermore, one can evaluate the moment of inertia through Eq. (18); the results are listed in Table 2. As in the case of the reference moment of inertia in Table 1, the calculated moment of inertia is always smaller by about 10%. The calculated angle θ_J is systematically smaller than $\theta_K(I)$, and accordingly the calculated $B(M1)/B(E2)$ ratio is systematically larger. This suggests that the calculation may be improved by including the quadrupole pairing interaction, which increases the moment of inertia and consistently reproduces the inertia and the even-odd mass difference [29]. The dot-dashed line in Fig. 4 is the calculated $B(M1)/B(E2)$ ratio by using the PAC formula (15) for $B(M1)$ value. Apparently, the PAC scheme underestimates the ratio considerably at lower frequency. This is because the effect of the geometry of the angular momentum vector (or of the Clebsch-Gordan coefficient in the strong-coupling expression) is not taken into account in the PAC model. However, at higher frequency the TAC result approaches to the PAC one, since the selfconsistent angle goes to 90° (aligned to the collective x -axis). In the case of ^{159}Dy the two calculations do not coincide at highest frequency. This is due to the fact that further alignments happen in the TAC calculation and so the two g -factors (16) and (21) deviate considerably.

² It was discussed in Ref. [23] that the TAC model gives a better result for the routhian of Band 2 in ^{155}Gd by comparing the experimental data with a simple CSM calculation, where the chemical potential was fixed by neighbouring ^{156}Gd nucleus and used for all bands. It has been found that the careful treatment of the chemical potential in this paper makes the agreement of Band 2 much better even in the PAC model.

³ In Ref [23], the first line of Eq.(2) contains a typographical error.

Finally, in order to study the dependence of the results on the monopole pairing correlations, the calculated band head frequencies ω_{BH} are shown as functions of neutron and proton pairing gaps in Fig. 5; the qualitative feature of the results are apparent from the relation between the ω_{BH} and the moment of inertia, Eq. (18). It is clear from the figure that the reduction of the pairing gaps gives better agreement with the experimentally deduced ω_{BH} . However, if ω_{BH} is fitted, the resultant pairing gaps are too small and we cannot obtain good agreements for the routhians. The factors 0.7 and 0.9 for neutron and proton pairing gaps are chosen to compromise the agreements of the routhians and the $B(M1)/B(E2)$ ratios. In addition, we have investigated the selfconsistent pairing calculations. The results show that the pairing gap reduces quite fast as increasing the rotational frequency and the two-neutron alignments (band-crossing) occurs at much lower frequency in contradiction to the data. In order to avoid this early alignments, one has to use larger force strength, which lead to the further reduction of moment of inertia. Then, as is clear from the consideration above, the band head frequency is considerably delayed and the agreement of the $B(M1)/B(E2)$ ratio becomes poor. Thus, a simultaneous reproduction of the routhians and the $B(M1)/B(E2)$ ratio seems to be difficult if one uses the selfconsistent pairing calculation. This is the main reason why we have used the constant pairing gaps with their values listed in Table 1.

4 Conclusions

The TAC method [8] has been applied to the strongly-coupled high- K band associated with the $\nu[505] \frac{11}{2}^-$ Nilsson orbital, which has been recently measured up to high-spin states in several nuclei around ^{155}Gd nucleus at JAERI. The results show reasonably good overall agreement with experimental observations for the energy spectra (routhians) and $B(M1)/B(E2)$ ratios at the same time. We have also investigated the same problem by using different models; the strong-coupling model without Coriolis coupling (the lowest order intensity relation), and the conventional cranking model (the PAC model):⁴ The relations between these models are also clarified. The simplest form of the strong-coupling model gives a good description to the $B(M1)/B(E2)$ ratios if the parameters are adjusted, but the calculated routhians deviate considerably from the observed ones at middle or higher frequencies, which clearly indicates the importance of the non-perturbative treatment of the Coriolis coupling effect. On the other hand, the conventional PAC model is capable to describe the routhians of high- K bands in almost the same quality as the TAC model, but the agreement for the $B(M1)/B(E2)$ ratios is poor at lower frequency, which is due to the deficiency that a proper geometry of the angular momentum vector with respect to the deformed-body are not taken into account. Thus, it is concluded that the TAC method is a simple and yet useful means to study strongly-coupled high- K rotational bands.

It should be mentioned that the result of the present TAC calculations is not very satisfactory. It is necessary to use the neutron and proton pairing gaps that are close to the even-odd mass differences in order to achieve a good overall agreement for all the routhians of negative and positive yrast bands as well as $\nu h_{11/2}$ high- K band. However, then the band head frequency for the high- K band is overestimated, which is quite sensitive to the pairing gaps used, and consequently the $B(M1)/B(E2)$ ratio is too large in the low frequency region. The sensitivity of the band head frequency is traced back to the sensitivity of the moment of inertia to the pairing gaps: Note that the monopole pairing, which reproduces the even-odd mass difference, gives too small moment of inertia. Thus, we believe that the inclusion of the quadrupole pairing interaction, which is known to remedy the problem of

⁴ Of course, the strong-coupling model and the TAC as well as PAC model are conceptually different: In the former it is not specified how to calculate the essential quantities like the moment of inertia or the quadrupole moment, while such quantities are microscopically calculable in the latter models.

small moment of inertia [29], will improve the agreement of both the routhians and $B(M1)/B(E2)$ ratio between the calculations and data. Such calculations are now in progress.

For the one-quasiparticle bands like the one considered in the present paper, other theoretical approaches are available, e.g. the particle-rotor model, or more sophisticated microscopic approach like the projected shell model [4], or the full angular momentum projection approach [3]. It is, however, increasingly more difficult to apply them to the case of multi-quasiparticle bands. Although the validity of the mean-field approximation should be always carefully checked, the TAC approach is relatively easy to apply for such more complicated rotational bands [8]. We would like to extend the present study by means of the TAC method to such cases in near future; e.g. to the rotational bands built on the high- K multi-quasiparticle states.

5 Acknowledgments

We are grateful to the nuclear spectroscopy group at JAERI for providing us experimental data before publications. Numerical calculations in this work were performed in part by using the computer system of Research Center for Nuclear Physics (RCNP), Osaka University, and the Yukawa Institute Computer Facility, Kyoto University. This work is supported in part by the Grant-in-Aid for Scientific Research from the Japan Ministry of Education, Culture, Sports, Science and Technology (No. 12640281).

References

- [1] Å. Bohr and B. Mottelson, *Nuclear Structure*, vol.II (Benjamin, New York, 1975).
- [2] P. Ring and P. Schuck, *The Nuclear Many-Body Problem*, (Springer-Verlag, 1980).
- [3] K. W. Schmid, F. Grümmer, and A. Faessler, *Ann. Phys.* **180** (1987), 1.
- [4] K. Hara and Y. Sun, *Int. J. Mod. Phys. E* **4** (1995) 637.
- [5] R. Bengtsson and S. Frauendorf, *Nucl. Phys.* **A327** (1979) 139.
- [6] J.D. Garrett, G.B. Hagemann and B. Herskind, *Ann. Rev. Nucl. Part. Sci.* **36** (1983) 419.
- [7] S. Frauendorf, *Nucl. Phys.* **A557** (1993) 259c.
- [8] S. Frauendorf, *Nucl. Phys.* **A677** (2000) 115.
- [9] S. Frauendorf, *Rev. Mod. Phys.* **73** (2001) 463.
- [10] R.M. Clark and A.O. Macchiavelli, *Annu. Rev. Nucl. Part. Sci.* **50** (2000) 1.
- [11] S. Frauendorf and J. Meng, *Z. Phys.* **A356** (1996) 263.
- [12] S. G. Nilsson and I. Ragnarsson, *Shapes and Shells in Nuclear Structure* (Cambridge University Press, 1995)
- [13] T. Bengtsson and I. Ragnarsson, *Nucl. Phys.* **A436** (1985) 14.
- [14] A. K. Kerman and N. Onishi, *Nucl. Phys.* **A361** (1981), 179.
- [15] I. Hamamoto and H. Sagawa, *Nucl. Phys.* **A327** (1979) 99.

- [16] M. Matsuzaki, Y.R. Shimizu, and K. Matsuyanagi, Prog. Theor. Phys. **79** (1988) 836.
- [17] Y. R. Shimizu and T. Nakatsukasa, Nucl. Phys. **A611** (1996) 22.
- [18] S.-I. Ohtsubo and Y.R. Shimizu, Prog. Theor. Phys. **98** (1997) 1099.
- [19] F. Dönau, Nucl. Phys. **A471** (1987) 469.
- [20] M. Oshima, M. Matsuzaki, S. Ichikawa, H. Iimura, H. Kusakari, T. Inamura, and A. Hashizume, Phys. Rev. **C40** (1998) 2084.
- [21] T. Hayakawa, M. Oshima, Y. Hatsukawa, J. Katakura, H. Iimura, M. Matsuda, N. Shinohara, Y. Toh, S. Mitarai, T. Shizuma, M. Sugawara, and H. Kusakari, Eur. Phys. J. **A9** (2000) 153.
- [22] J. Rekstad, M. Guttormsen, T. Engeland, G. Løvholden, O. Straume, J. Lien, and C.E. Ellegaard, Nucl. Phys. **A320** (1979) 239.
- [23] T. Hayakawa, M. Oshima, Y. Hatsukawa, J. Katakura, H. Iimura, M. Matsuda, S. Mitarai, Y.R. Shimizu, S.-I. Ohtsubo, T. Shizuma, M. Sugawara, and H. Kusakari, Nucl. Phys. **A657** (1999) 3.
- [24] H. Kusakari, M. Oshima, A. Uchikura, M. Sugawara, A. Tomotani, S. Ichikawa, H. Iimura, T. Morikawa, T. Inamura, and M. Matsuzaki, Phys. Rev. **C46** (1992) 1257; **C63** (2001) 029901(E).
- [25] T. Hayakawa, *et al.*, private communication.
- [26] M. Sugawara, S. Mitarai, H. Kusakari, M. Oshima, T. Hayakawa, Y. Toh, Y. Hatsukawa, J. Katakura, H. Iimura, Y.H. Zhang, M. Sugie and Y. Sato, Nucl. Phys. **A699** (2002) 450.
- [27] <http://www.nndc.bnl.gov/>, National Nuclear Data Center, Brookhaven National Laboratory.
- [28] S. G. Nilsson and O. Prior, Mat. Fys. Medd. Dan. Vid. Selsk. **32** (1961) no.16.
- [29] Y.R. Shimizu and K. Matsuyanagi, Prog. Theor. Phys. Suppl. **141** (2001) 285.
- [30] Å. Bohr and B. Mottelson, *Nuclear Structure*, Vol.I (Benjamin, New York, 1969).
- [31] T. Kutsarova, R. M. Lieder, H. Schnare, G. Hebbinghaus, D. Balabanski, W. Gast, A. Krämer-Flecken, M. A. Bently, P. Fallon, D. Howe, A. R. Mokhtar, J. F. Sharpey-Schafer, P. Walker, P. Chowdhury, D. Fabricius, G. Sletten and S. Frauendorf, Nucl. Phys. **A587** (1995) 111.

Nuclei	ϵ_2	ϵ_4	Δ_ν [MeV]	Δ_π [MeV]	\mathcal{J}_0 [\hbar^2 /MeV]	
					Experiment	Calculation
^{153}Sm	0.254	-0.0373	0.814	0.918	29.4	26.5
^{155}Gd	0.256	-0.0279	0.821	0.942	29.2	26.3
^{157}Gd	0.258	-0.0300	0.687	0.827	34.6	31.4
^{157}Dy	0.256	-0.0181	0.821	0.988	27.8	25.0
^{159}Dy	0.257	-0.0202	0.715	0.905	31.4	28.3

Table 1: Deformation parameter, pairing gap and the moment of inertia of the reference band used in the calculation.

	Nuclei	^{153}Sm	^{155}Gd	^{157}Gd	^{157}Dy	^{159}Dy
$\mathcal{J}_{K=11/2}$	Experimental	44.2	40.2	47.8	37.0	40.1
	Calculation	35.7	35.9	41.9	33.0	37.4

Table 2: Moment of inertia (in \hbar^2 /MeV) estimated from the experimental and calculated band head frequency through Eq. (18) for the $\nu[505]\frac{11}{2}^-$ band.

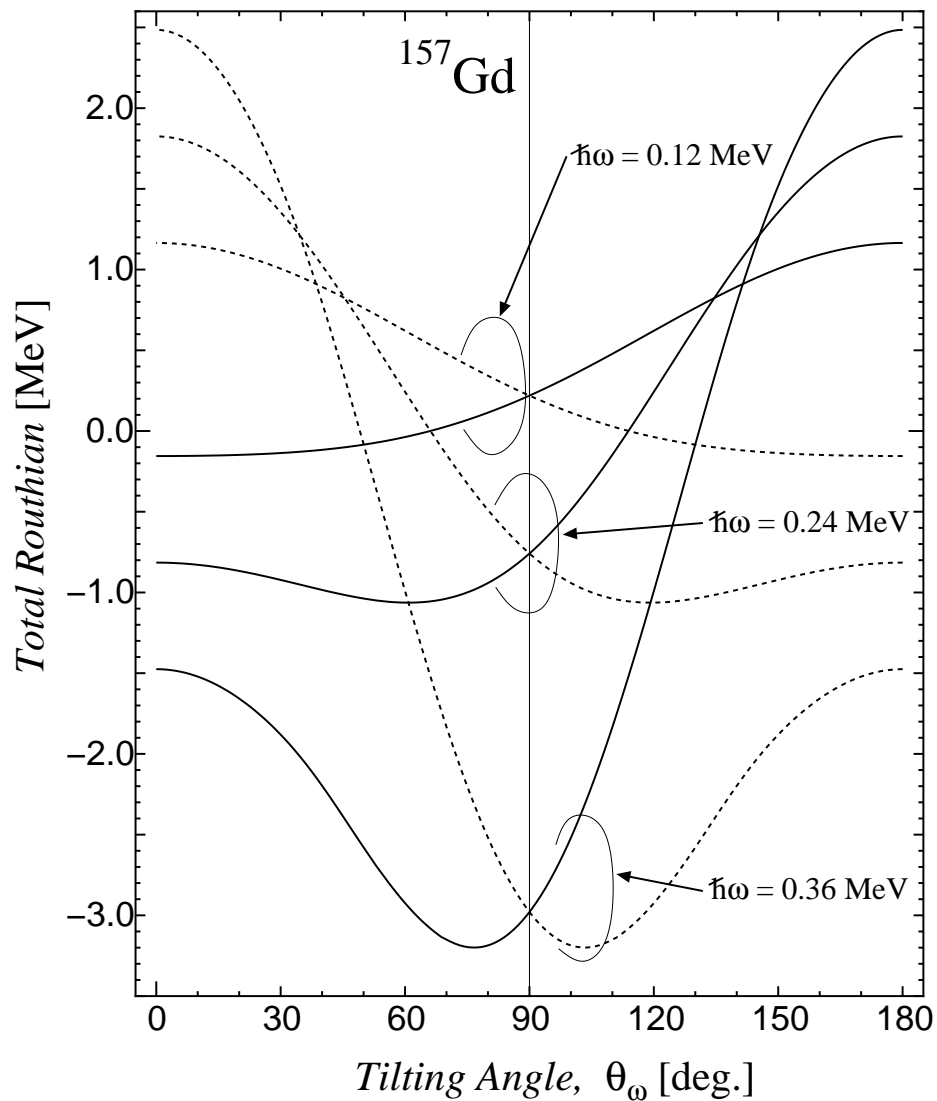


Figure 1: The total routhians calculated for the $\nu[505]11/2^-$ configuration (high- K band) in ^{157}Gd are shown as functions of the tilting angle θ_ω . Three pairs of solid and dashed curves are the ones at the rotational frequency, $\hbar\omega = 0.12, 0.24$ and 0.36 MeV. Two curves denoted by the solid and dotted line are connected diabatically starting from the $\theta_\omega = 0^\circ$ and $\theta_\omega = 180^\circ$, respectively.

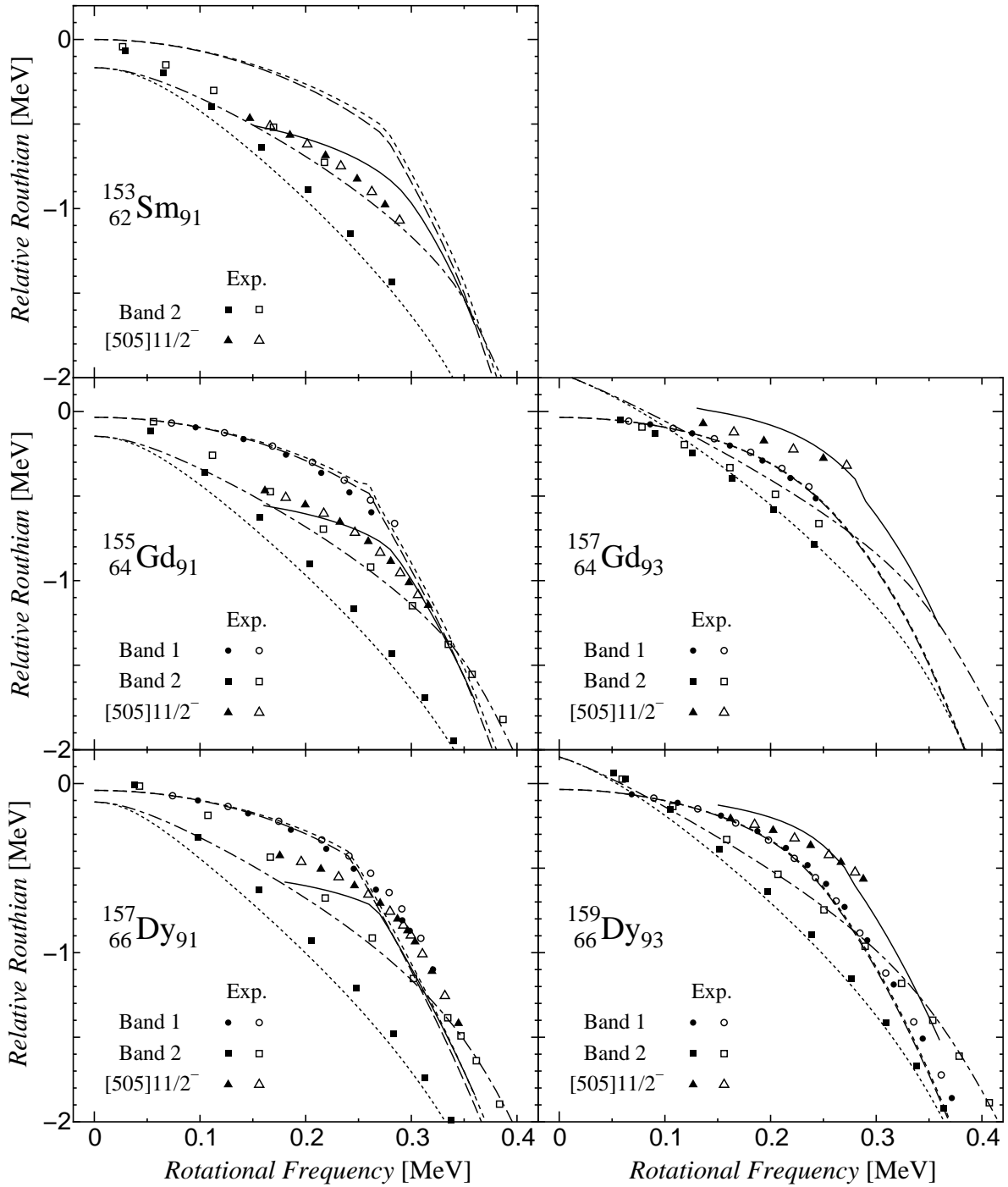


Figure 2: Comparison of the calculated and experimental routhians as functions of the rotational frequency in ^{153}Sm , $^{155,157}\text{Gd}$ and $^{157,159}\text{Dy}$ nuclei. The long-dashed and short-dashed lines denote calculated routhians with signature $\alpha = +1/2$ and $-1/2$ for the positive-parity yrast band (Band 1), the dotted and dot-dashed lines denote calculated routhians with signature $\alpha = +1/2$ and $-1/2$ for the negative-parity yrast band (Band 2), and the full line denotes the calculated routhian for the high- K , $\nu[505]_{1/2}^-$ band. The filled and open circles denote experimental routhians with signature $\alpha = +1/2$ and $-1/2$ for Band 1, the filled and open squares denote experimental routhians with signature $\alpha = +1/2$ and $-1/2$ for Band 2, and the filled and open triangles denote experimental routhians with signature $\alpha = +1/2$ and $-1/2$ for the high- K band. The “rigid-body” reference routhian, $-\frac{1}{2}\mathcal{J}_0\omega^2$, is subtracted. Here the values of \mathcal{J}_0 used for the experimental and calculated routhians are different and listed in Table 1.

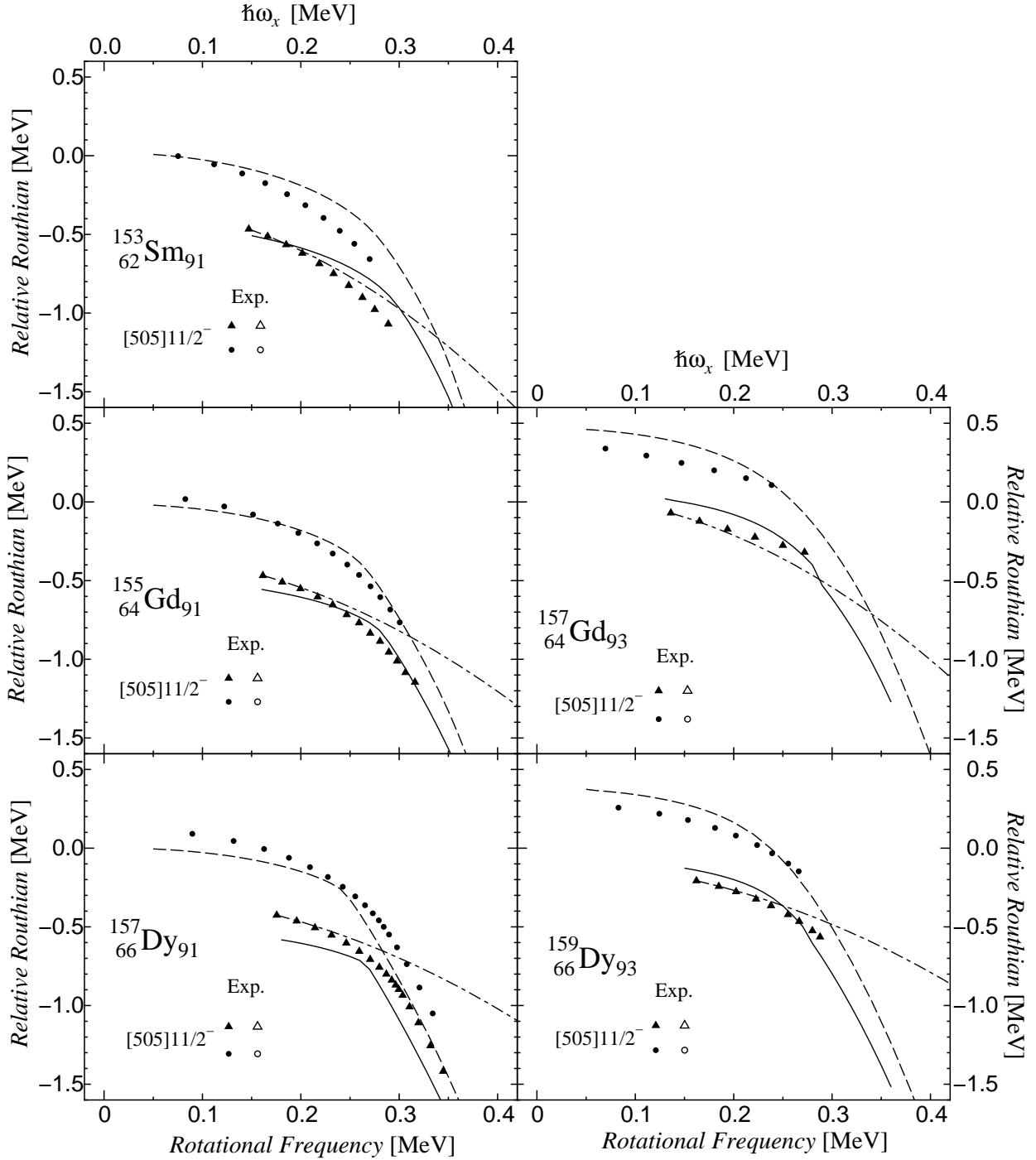


Figure 3: Comparison of the calculated (lines) and experimental (symbols) routhians for the $\nu[505]\frac{11}{2}^-$ band. The full lines and the triangles denote the TAC scheme routhians, $E'(\omega)$, c.f. Eq. (7), while the dashed lines and the circles denote the PAC scheme routhians, $E'_x(\omega_x)$, c.f. Eq. (23). The dot-dashed lines also denote the calculated TAC scheme routhians, but using the strong-coupling expression (24), where the used parameters are $K = 11/2$, \mathcal{J} listed in Table 2, and E_K^{0l} adjusted to fit the data at the lowest frequency for each nucleus.

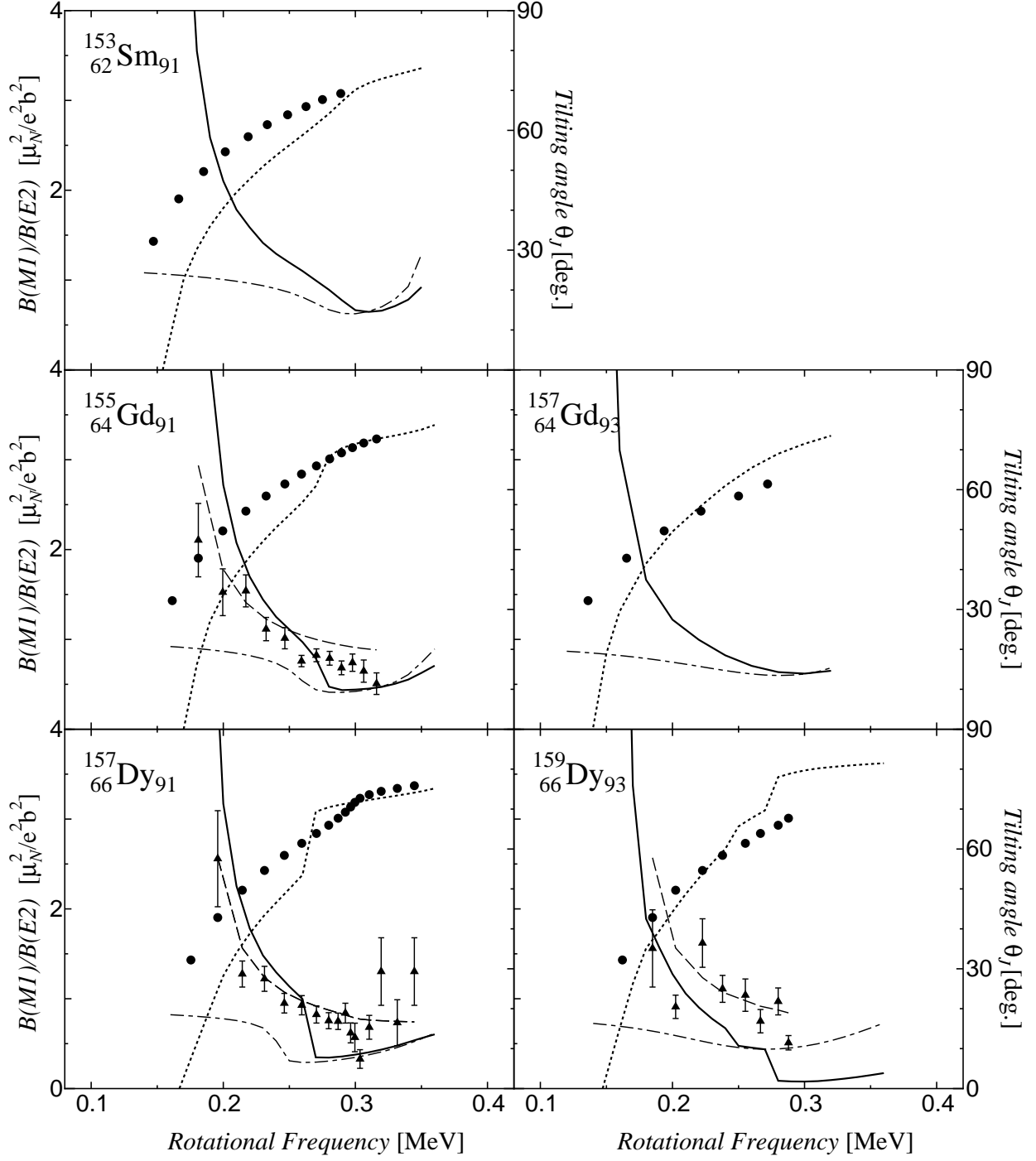


Figure 4: Comparison of the calculated and experimental $B(M1)/B(E2)$ ratios for the $\nu[505]_{11/2}^-$ band as functions of the rotational frequency in ^{153}Sm , $^{155,157}\text{Gd}$ and $^{157,159}\text{Dy}$ nuclei. The solid and dot-dashed lines denote the results by using the TAC and PAC models, respectively. The dashed line denotes the result of the strong-coupling formula (25), where the parameter $[(g_K - g_R)K/Q_0]^2$ is adjusted to fit the data for each nucleus. The triangles with error bar denote the experimental ratios. In this figure, the selfconsistently determined tilting angle θ_J and the experimentally deduced angle (17) are also included as dotted lines and circles, respectively; the scale for them is shown on the right hand side.

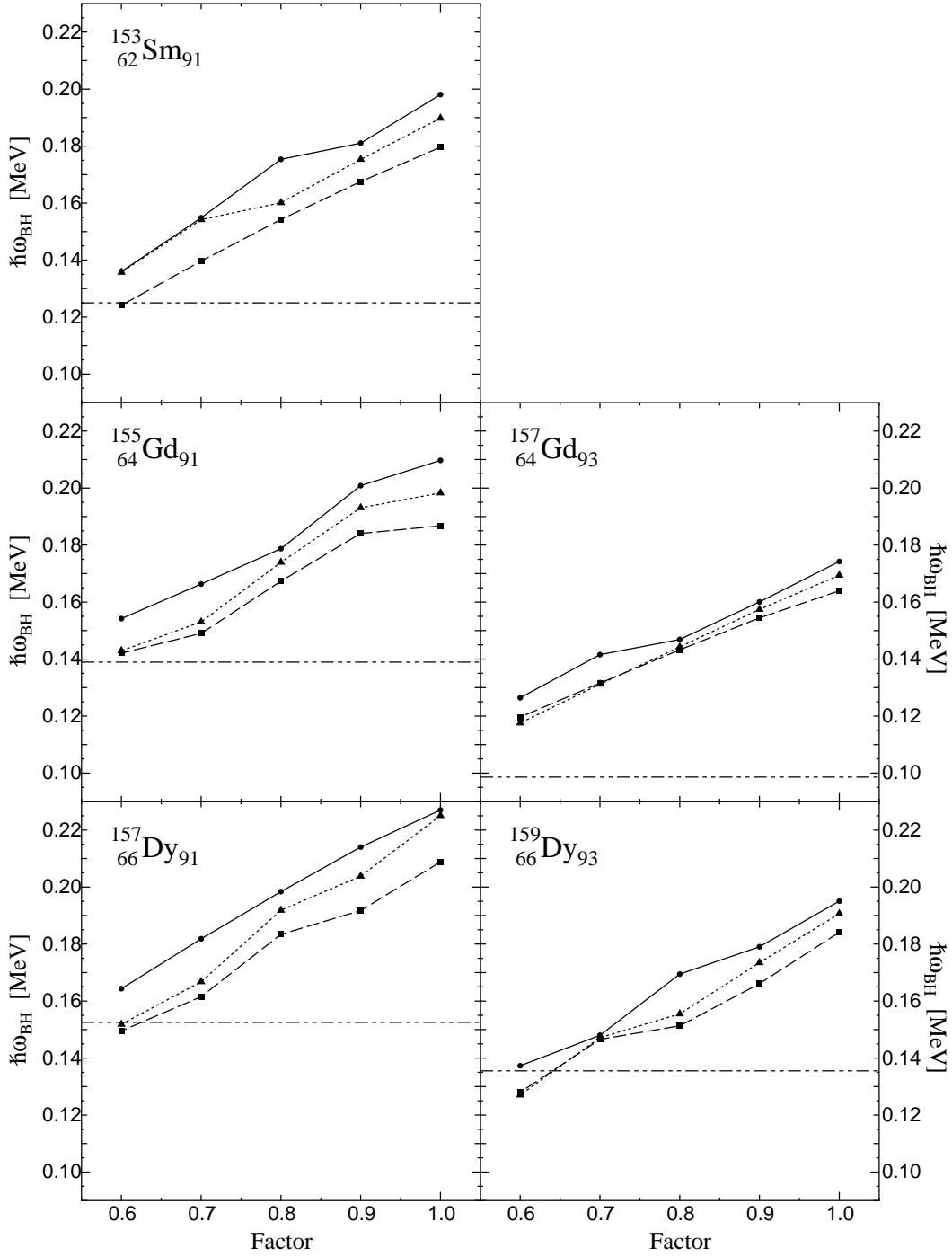


Figure 5: Dependence of the band head frequency ω_{BH} on the neutron and proton pairing gap parameters in ^{153}Sm , $^{155,157}\text{Gd}$ and $^{157,159}\text{Dy}$ nuclei. Here ω_{BH} has been obtained by the TAC calculation where are used the neutron and proton pairing gaps whose values are determined by multiplying the even-odd mass differences by some factors. Thus calculated ω_{BH} is shown as a function of the factor of neutron gap. The solid lines with circles, dotted lines with triangles, and dashed lines with squares denote the results with the factor of proton gap being 1.0, 0.9, and 0.8, respectively.